Biochimica et Biophysica Acta 1828 (2013) 632–641

Contents lists available at SciVerse ScienceDirect

Biochimica et Biophysica Acta

journal homepage: www.elsevier.com/locate/bbamem

Porter domain opening and closing motions in the multi-drug efflux transporter AcrB

Nadine Fischer, Christian Kandt *

Computational Structural Biology, Department of Life Science Informatics, B-IT, Life & Medical Sciences (LIMES) Institute, University of Bonn, Dahlmannstr 2, 53113 Bonn, Germany

ARTICLE INFO

Article history:
Received 16 March 2012
Received in revised form 2 October 2012
Accepted 13 October 2012
Available online 23 October 2012

Keywords:
Molecular dynamics simulation
Membrane protein
Antibiotics resistance
Proximal binding pocket
Hydrophobic binding pocket
Reaction cycle

ABSTRACT

Acriflavine resistance protein B acts as the active transporter in the multi-drug efflux pump Acriflavine resistance proteins A / B - Tolerance to colicins protein in *Escherichia coli*. Within the same reaction cycle intermediate all Acriflavine resistance protein B X-ray structures display highly similar conformations of the substrate-recruiting and transporting porter domain. To assess if this structural homogeneity is an intrinsic feature of Acriflavine resistance protein B or stems from other causes we performed a series of six independent, unbiased 100 ns molecular dynamics simulations of membrane-embedded, asymmetric, substrate-free wild type Acriflavine resistance protein B in a 150 mM NaCl solution. We find the porter domain more flexible than previously assumed displaying clear opening and closing motions of the proximal binding pocket (L and T-state) and the exit of the drug transport channels (O-intermediate). Concurrently the hydrophobic binding pocket favors a closed conformation in all three protomers. Our findings suggest that the conformational homogeneity seen in the crystal structures is likely an effect of bound but structurally unresolved substrate. Our simulations further imply that each of the known three reaction cycle intermediates occurs in at least two variants, the Thr676 loop independently regulates porter domain access and likely plays a key role in substrate transport. On a 100 ns time scale we find no evidence supporting the proposed LLL resting state in the absence of substrate. If the proximal binding pocket dynamics have an inhibiting effect on Acriflavine resistance protein B pump activity lowering the life time of substrate-accessible conformations, the observed dynamics could provide a structural explanation for the Acriflavine resistance protein B activity-enhancing effect of the adaptor protein Acriflavine resistance protein A stabilizing PC1 and PC2 subdomain orientations.

1. Introduction

Preventing drug access to the target molecule is one of the main ways by which bacteria achieve multi-drug resistance [1,2]. In Gram-negative bacteria a prominent example for this mechanism of action is an overproduction of multi-drug efflux pumps of the resistance nodulation division (RND) protein super family such as AcrAB-TolC [3] (Fig. 1a). Combining three different protein components, AcrAB-TolC comprises the outer membrane efflux duct TolC [4], the inner membrane-anchored adaptor protein AcrA [5] and the inner membrane transporter Acriflavine resistance protein B (AcrB) acting as engine of the assembled pump [6–8]. Converting the energy of proton gradient over the inner membrane into a cyclic sequence of conformational changes [9–12], AcrB transports a broad variety of substrates from periplasmic space out of the cell.

Whereas proton conduction takes place in the AcrB trans-membrane domain (TMD), substrate recruitment and transport occur in the porter domain (PD) (Fig. 1b) [13] where the "Phe617"/"switch loop" divides the transport channels into an outer "access"/"proximal binding pocket" and an inner "deep"/"distal"/"hydrophobic binding pocket" (HBP) [9,14–16] from where substrates are transported towards the central funnel formed by the AcrB docking domain (DD) (Fig. 1). Entrance (PDe) and exit (PDx) of the porter domain substrate transport channels have been found trapped in monomer-specific states of substrate accessibility in recent AcrB crystal structures (Fig. 1c,d) [9,14,17]. Whereas in monomers A and B – proposed as "*L*oose/access" and "*T*ight/binding" intermediates in the AcrB reaction cycle [9,14,17] – the transport channels exhibit open PDe/proximal binding pocket but closed PDx conformations, in monomer C – the "*O*pen/extrusion" reaction cycle intermediate – PDe is closed but PDx is open. Whether other conformational states besides the known X-ray intermediates occur in the AcrB reaction cycle is currently unknown. However, combined mutagenesis and mass spectrometry experiments introducing engineered disulfide bonds reported that while conformational transitions between L (monomer A) and T (monomer B) protomers occur in vivo, there is never more than one monomer displaying the O (monomer C) conformation [11].

At the time of writing a total of 33 different AcrB crystal structures have been published. Of these 19 structures are in a three-fold symmetric form showing identical monomer conformations representing the L state [18–25], whereas in 14 structures each monomer was trapped in a different conformation representing the LTO reaction cycle intermediates [9,14–17]. Remarkably, when comparing the PD conformation of these structures using Cα root mean square displacement after least squares fitting to the asymmetric and ligand-free 2GIF AcrB X-ray structure [9] – which we used as starting structure for our molecular dynamics (MD) simulations – all structures are very similar, displaying Cα-RMSDs of less than 0.1 nm for each

* Corresponding author. Tel.: +49 228 2699 324; fax: +49 228 2699 341.
E-mail address: kandt@bit.uni-bonn.de (C. Kandt).

0005-2736/$ – see front matter © 2012 Elsevier B.V. All rights reserved.
http://dx.doi.org/10.1016/j.bbamem.2012.10.016

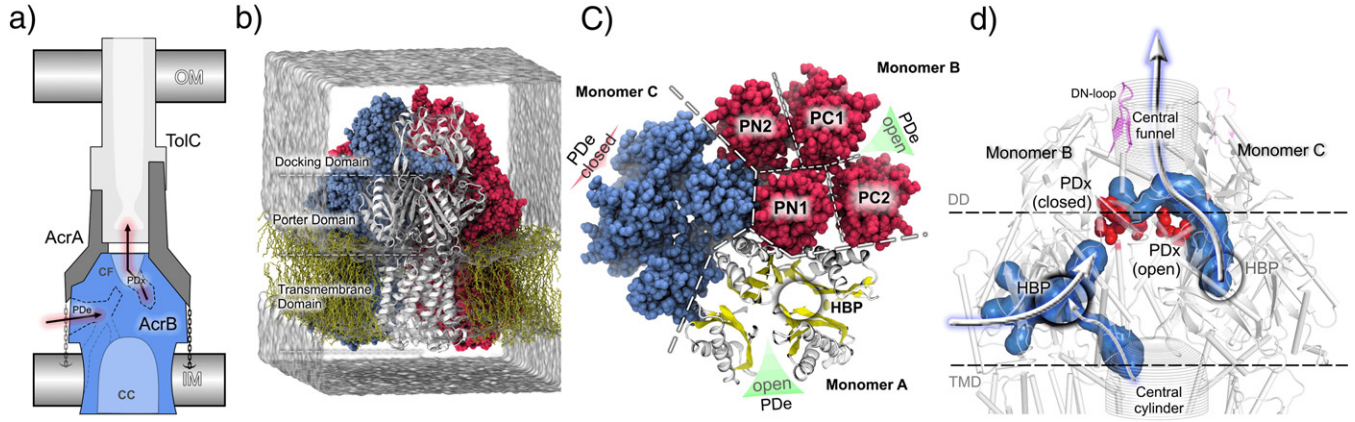

Fig. 1. Simulation system and porter domain accessibility. Embedded in the inner cell membrane (IM) AcrB acts as active transporter in the tripartite AcrAB–TolC multidrug efflux pump transferring a broad range of substrates towards TolC via the central funnel (CF) in AcrB docking domain (a). Here we report molecular dynamics simulation of asymmetric 2GIF AcrB in a phospholipid membrane/water environment at a 150 mM NaCl concentration (b). Monomer asymmetry is mainly based on different conformations of the porter domain (PD). Monomers A and B exhibit a large periplasmic cleft between PC1 and PC2 subdomains marking the main entrance PDe of the substrate transport channel, which is closed in monomer C (b). Conversely, the exit of the transport channel PDx is open only in monomer C. Resultant different accessibilities of the porter domain are highlighted by monomer-internal tunnel-like cavities as detected by Caver 2.0 [55] (c).

monomer (Fig. 2). Whether this high conformational similarity represents an intrinsic feature of AcrB or originates from other causes is currently not known.

So far computational investigations of AcrB have focused on assessing conformational flexibility via normal mode analyses [26], coarse-grained molecular dynamics (MD) studies of isolated protein sections [27], simulating conformational transitions using targeted MD techniques [28–30], as well as predicting water distribution and dynamics in the energy-converting trans-membrane domain based on which three possible proton conduction pathways were derived [31]. Here we report molecular dynamics simulations of asymmetric AcrB addressing the question why all available crystal structures show very similar, monomer-characteristic PD conformations. To provide evidence whether this high level of conformational homogeneity represents an intrinsic feature of the protein or could be related to AcrB crystallization conditions, we simulated wild-type, substrate-free AcrB [9] in a close-to-native, phospholipid membrane/water environment at 150 mM NaCl concentration to obtain samples of unrestrained wild type AcrB dynamics outside a crystal environment in a series of six unbiased and independent MD runs each 100 ns long. As in our previous work [31] standard protonation states were assumed for titratable except for the known key residues of proton conductance Asp407, Asp408, Lys940 and Arg971 which were protonated monomer-specifically according to [10].

Using distance, cross-sectional area and radius of gyration analyses to monitor the PDe, PDx and HBP opening state in each monomer, we find that the porter domain is more flexible than previously assumed displaying clear opening and closing motions of the proximal binding pocket in the L and T states as well as in the exit region of the drug transport channels in the O intermediate supporting the hypothesis of Gln125 and Tyr758 acting as gating residues [17]. Concurrently in all simulations the hydrophobic binding pocket collapses in the T monomer resulting in predominantly closed HBP conformations in all three protomers. Comparing our protein conformations to AcrB X-ray structures our findings

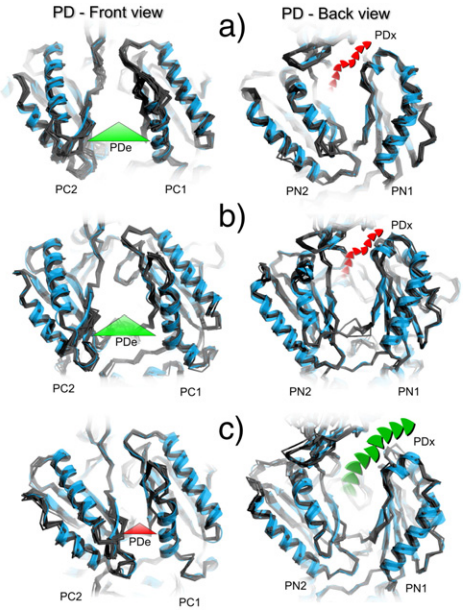

Symmetric AcrB		Asymmetric AcrB			
PDB-ID	RMSD (Å)	PDB-ID	A	B	C
1IWG	0.642	2DHH	0.491	0.498	0.560
1OY6	0.651	2DR6	0.536	0.572	0.570
1OY8	0.661	2DRD	0.461	0.506	0.559
1OY9	0.686	2J8S	0.680	0.514	0.423
1OYD	0.710	3AOA	0.462	0.448	0.564
1OYE	0.686	3AOB	0.412	0.392	0.532
1T9T	0.697	3AOC	0.464	0.442	0.516
1T9U	0.713	3AOD	0.393	0.372	0.506
1T9V	0.707	3NOC	0.440	0.667	0.410
1T9W	0.748	3NOG	0.816	0.779	0.817
1T9X	0.727	4DX5	0.350	0.427	0.385
1T9Y	0.728	4DX6	0.482	0.504	0.430
2HQC	0.680	4DX8	0.404	0.407	0.366
2HQD	0.703	2HRT	0.244	0.238	0.237
2HQF	0.654				
2HQG	0.602				
2I6W	0.638				
2W1B	0.735				
2RDD	0.680				
3D9B	0.537				
Av.	0.683	Av.	0.488	0.474	0.491

Fig. 2. Comparison of AcrB crystal structures. Superimposing the available 33 X-ray structures using the porter domain (PD) α-carbons of the 2GIF X-ray as reference (blue) it becomes evident, that all crystal structures display nearly identical PD conformations in the same reaction cycle intermediate with Ca root mean square displacements below 0.1 nm. Green and red arrows mark open and closed PDe and PDx conformations.

suggest that the conformational homogeneity seen in the crystal structures is likely not an intrinsic feature of the protein but an artifact caused by bound but structurally unresolved buffer or detergent molecules. The observed PDe and PDx dynamics further imply that each of the currently known three reaction cycle intermediates can occur in at least two variants and that beyond independently regulating porter domain access the Thr676 loop connecting the PC1 and PC2 subdomains could play a key role in substrate transport pushing compounds towards the hydrophobic binding pocket. On a 100 ns time scale we observe no conformational trends supporting the hypothesis of a homogeneous LLL AcrB resting state in the absence of substrate [22]. If the proximal binding pocket dynamics have an inhibiting effect on AcrB pump activity by lowering the life time of substrate-accessible conformations, the observed opening and closing motions in the isolated protein could provide a structural explanation for the AcrB activity-enhancing effect of the adaptor protein AcrA [7] stabilizing substrate-accessible porter domain conformations.

2. Materials and methods

2.1. Molecular dynamics simulations

6×100 ns independent and unbiased molecular dynamics simulations were carried out using GROMACS 4.0.3 [32,33] and the GROMOS96 53a6 force field [34]. As detailed in [31] the asymmetric AcrB crystal structure 2GIF [9] was inserted in a pre-equilibrated 14×14 nm, 457 lipid palmitoyloleoyl-phosphatidylethanol-amine (POPE) bilayer [35] and subsequently solvated in a 150 mM NaCl solution of 273 sodium ions, 230 chloride ions and 49521 simple point charge water molecules [36] (Fig. 1a). Except for Asp407, Asp408, Lys940 and Arg971, which were protonated monomer-specifically according to [10], standard protonation states were selected for titratable residues. After an initial period of 30 ns membrane equilibration – with all non-hydrogen protein atoms position-restrained applying a force constant of 1000 kJ/(mol nm^2) – production runs were initiated using different random seed numbers to generate the distributions of starting velocities. A temperature of 310 K was maintained separately for protein, lipids and water+ions by a Berendsen thermostat [37] with a time constant of $\tau_T = 0.1$ ps. Semi-isotropic pressure coupling was employed using a Berendsen barostat [37] with time constants of 4 ps and reference pressures of 1 bar in Z and XY direction. Electrostatic interactions were calculated using particle mesh Ewald summation [38,39], and twin range cut-offs of 1.0 and 1.4 nm were applied for computing the van der Waals interactions. In all simulations bond lengths were constrained by LINCS [40] to permit an integration time step of 2 fs.

2.2. Analysis

2.2.1. Crystal structure comparison

All 33 currently available AcrB crystal structures were compared computing the porter domain Cα root-mean square deviations (RMSD) after least squares fitting to the porter domain of the asymmetric and ligand-free 2GIF AcrB X-ray structure [9]. Structural alignment and RMSD calculation were carried out in PyMOL 1.5 using the α-carbons of residues 36–130, 137–178, 276–326, 567–666, 678–722 and 813–860. As symmetric AcrB crystal structures [18–25] represent the monomer A (loose/binding) conformation 2GIF monomer A was used as fitting reference for the symmetric AcrB structures, whereas the asymmetric AcrB X-ray structures [9,14–17] were superimposed on 2GIF using the corresponding monomer pairings.

2.2.2. Protein stability, conformational sampling and average structure

To assess protein stability we computed Cα RMSDs separately for each AcrB monomer and its trans-membrane, porter and docking domains after respective least squares fitting to the starting structure. To assess the overall amount of conformational sampling throughout the simulations, a principal component analysis was performed on the PD-DD α-carbons using the GROMACS tools g_covar and g_anaeig projecting for each run AcrB's pathway through conformational space onto the first three Eigenvectors. The simulation average structure was determined based on the last 60 ns of each trajectory using an iterative scheme of calculating the average conformation and re-aligning the trajectory to that average structure to compute a new average structure until the average conformation stopped changing.

2.2.3. Porter domain accessibility

Accessibility of the AcrB porter domain was monitored focusing on the entry and exit regions of the transport channels. Using the GROMACS tool g_mindist the opening state of the channel entrances was determined calculating the number of Cα–Cα contacts between entrance-flanking PC1 and PC2 sub-domains within a distance range of 1 nm. For each run and monomer the minimum distance data was subsequently processed into three classes of less, identical (±1) or more inter-domain contacts as the 2GIF crystal structure (exhibiting 5 contacts in monomer A, 8 in B and 45 in C). Furthermore the overall distribution of Cα-contacts was computed over all six simulations and compared to the 2GIF crystal structure. In addition to that the intermediate-specific conformation of the Thr676 loop connecting the PC1 and PC2 subdomains were monitored using g_dist to calculate for each monomer the Thr676–Phe563 Cα-distance distribution over all six simulations.

The opening state of the channel exits was monitored calculating the center of mass (COM) distance between the proposed gating residues Gln124 and Tyr758 [17] using the GROMACS tool g_dist. Resulting distance data were subsequently grouped into three classes exhibiting smaller, identical (±0.1 nm) or larger COM-distances as in the 2GIF X-ray structure (0.56 nm in monomer A, 0.48 nm in B and 1.14 nm in C). Additionally, the overall distribution of Gln124–Tyr758 COM-distances was computed over all six simulations and compared to the 2GIF X-ray structure. In addition to that and similar to [41,42], the PDx opening state was monitored calculating the triangular cross-sectional area (TCA) spanned by the COMs of Gln124, Tyr758 and Pro50. Subsequently the area data was grouped into three classes displaying smaller, identical (±0.05 nm^2) or larger TCA as the 2GIF X-ray structure (0.24 nm^2 TCA in monomer A, 0.2 nm^2 TCA in B and 0.49 nm^2 TCA in C). Finally the overall TCA distribution was computed over all six simulations and compared to the 2GIF crystal structure.

2.2.4. Opening state of the hydrophobic binding pocket

In the crystal structures the hydrophobic binding pocket (HBP) displays an open conformation in monomer B but is closed in monomers A and C [9,14–17]. To monitor the opening state of the hydrophobic binding pocket throughout the simulations we computed the radius of gyration of the HBP residues Phe178, Phe610, Val139, Phe136, Tyr327, Phe628, Phe617, Iso626, Phe615, Val612 and Iso277. Employing the GROMACS tool g_gyrate the calculation was performed for each monomer using the HBP α-carbons to focus on large scale conformational changes only eliminating the influence of side chain fluctuations for a better signal to noise ratio.

2.2.5. Potential convergence of monomer conformations

To assess whether the absence of substrate leads to converging monomer conformations during the simulations we computed relative Cα RMSDs for all possible monomer combinations A vs. B, A vs. C and B vs. C and computed the Cα distance distribution between Ser562 and Thr837 in all monomers. Relative conformational differences between the monomers were quantified via PD-DD Cα-RMSDs using the respective monomers C and A conformation in each simulation frame as fitting reference. To assess whether the relative orientation of TMD-Ser562 and PD-Thr837 would permit the formation of a disulfide bond when

mutated to Cysteine which has been found indicative for the monomer C conformation [11], we computed the distribution of Ser562–Thr837 Cα distances over all simulations. Based on the average upper Cα distance limit of protein disulfide bonds reported in [43], disulfide bond formation was regarded possible at distances ≤0.638 nm.

3. Results

3.1. Protein stability and conformational sampling

In any molecular dynamics simulation the protein will undergo conformational changes increasing the conformational distance to its starting structure which is commonly monitored using α-carbon root mean square displacements (RMSD). When multiple MD simulations are performed the protein ideally explores different regions of conformational hyperspace around the X-ray structure in each independent run. To assess protein stability, we calculated for each AcrB monomer Cα RMSDs of the entire subunit as well as its transmembrane, porter and docking domain after respective least squares fitting to the X-ray starting structure (Fig. 3a). After 100 ns subunit-RMSDs range from 0.25 nm in monomer C to 0.35 nm in monomers A and B (Fig. 3a Protomers). Except for monomer C in two simulations all monomer RMSDs level after 20 ns; however all RMSD curves keep increasing throughout the simulation time. On TMD level the initial rapid RMSD increase is over after 3–10 ns; the RMSDs range from 0.17 nm (monomer C) to 0.34 nm (monomer A); and all runs have reached plateau levels after 70 ns (Fig. 3a, TMD). Leveling after 20 ns the PD-RMSDs range from 0.2 nm (monomer C) to 0.34 nm (monomer C) reaching plateaus after 45 ns in 5 monomer B and 3 monomer A simulations as well as after 35 ns in 4 monomer C runs (Fig. 3a, PD). Except for one monomer B simulation, exhibiting an end RMSD of 0.39 nm due to conformational change of the DN-top loop (Fig. 1d, magenta), all other simulations display a RMSD range between 0.22 and 0.32 nm after an initial rapid RMSD increase during the first 30 ns (Fig. 3a, DD).

To assess the overall amount of protein conformational sampling achieved during our simulations we carried out a principal component analysis of the PD and DD α-carbons. A common way to visualize the protein's path through high-dimensional conformational hyperspace is projecting it down onto the first three Eigenvectors describing the largest extent of conformational space sampled. As shown in Fig. 3b, where each dot represents a single protein conformation, AcrB samples different regions of conformational space in each of the six simulations indicating a high sampling quality obtained in the simulations.

3.2. Porter domain accessibility

Porter domain accessibility was analyzed focusing on the entrance PDe and exit regions PDx of the substrate transport channels (Fig. 1c,d) calculating inter-subdomain minimum distance contacts, distances and triangular cross-sectional areas of selected residues.

3.2.1. Substrate channel entrance PDe

To analyze the opening state of the entrance region of the PD substrate transport channels we monitored the amount of PC1–PC2 subdomain Cα–Cα contacts within 1 nm. The initial time-resolved data were subsequently processed computing (a) percentage per-run occurrences of conformations displaying more, similar or less contacts as the 2GIF crystal structure (Fig. 4a); (b) the overall distributions of sub-domain contacts calculated over all six simulations (Fig. 4b, Table 1) as well as (c) simulation snapshots of extreme conformations for each monomer based on the overall contact distribution (Fig. 4c). We find that channel entrances are dynamic, exhibiting in each monomer amounts of PC1–PC2 contacts that are predominantly higher or lower than in the 2GIF crystal structure. Extreme conformations derived from the overall distributions (Fig. 4c) imply that the range of inter-subdomain contacts (0–45 in A, 0–24 in B and 7–80 in C) includes opening and closing motions of PC1 and PC2 leading to PDe conformations both accessible and inaccessible for substrate in monomers A and B but not in C.

Although displaying a wide range of inter-subdomain contacts (Fig. 4b), the PDe in monomer C remains inaccessible for substrate in all simulations (Fig. 4c). To identify the structural basis for this behavior we analyzed the conformation of the Thr676 loop connecting the PC1 and PC2 subdomains. Whereas in the crystal structure the loop is in a conformation displaying membrane-facing Thr676 orientation in monomers A and B permitting substrate passage, in monomer C the loop adopts a different conformation where Thr676 has moved 1 nm towards the switch loop in monomer C, blocking substrate access (Fig. 5a). Monitoring the loop orientation through the

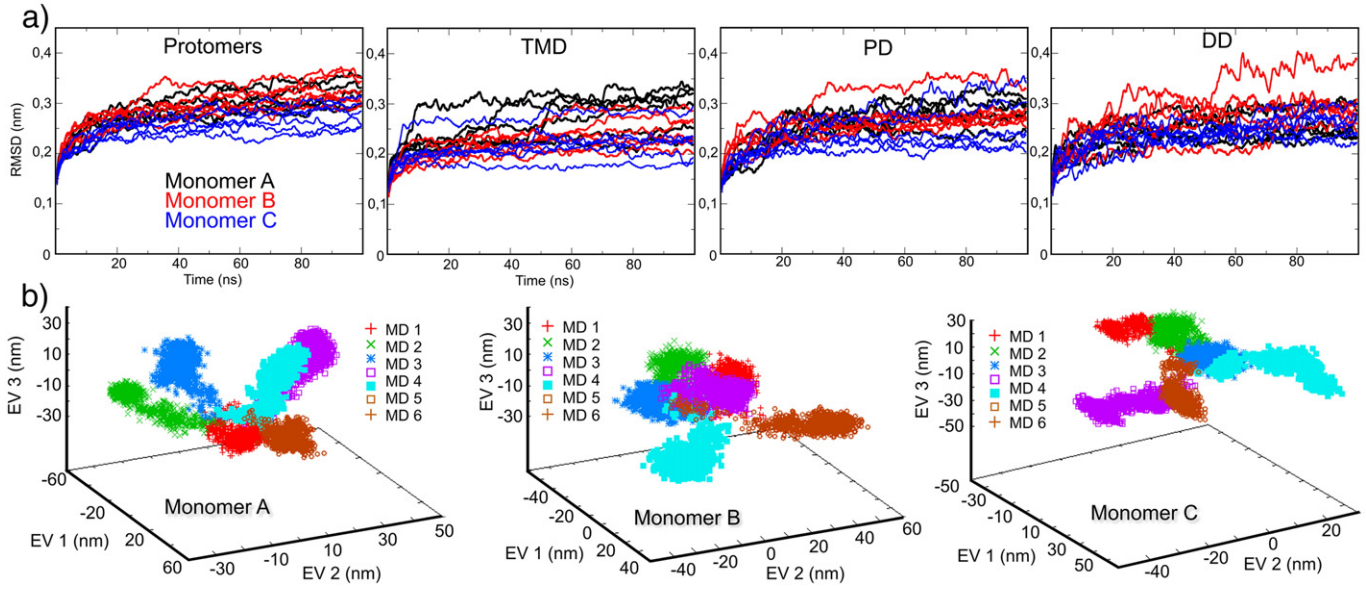

Fig. 3. Protein stability and conformational sampling. To assess protein stability in our simulations we calculated Cα root-mean square deviations of the entire AcrB monomers, trans-membrane domains (TMD), porter domains (PD) and docking domains (DD) after respective least squares fitting to the crystal structure (a). To estimate the amount of conformational sampling achieved in the simulations we determined in a principal component analysis of the porter and docking domain α-carbons each monomer's path through conformational space and projected it down to three dimensions spanned by the first three Eigenvectors (b).

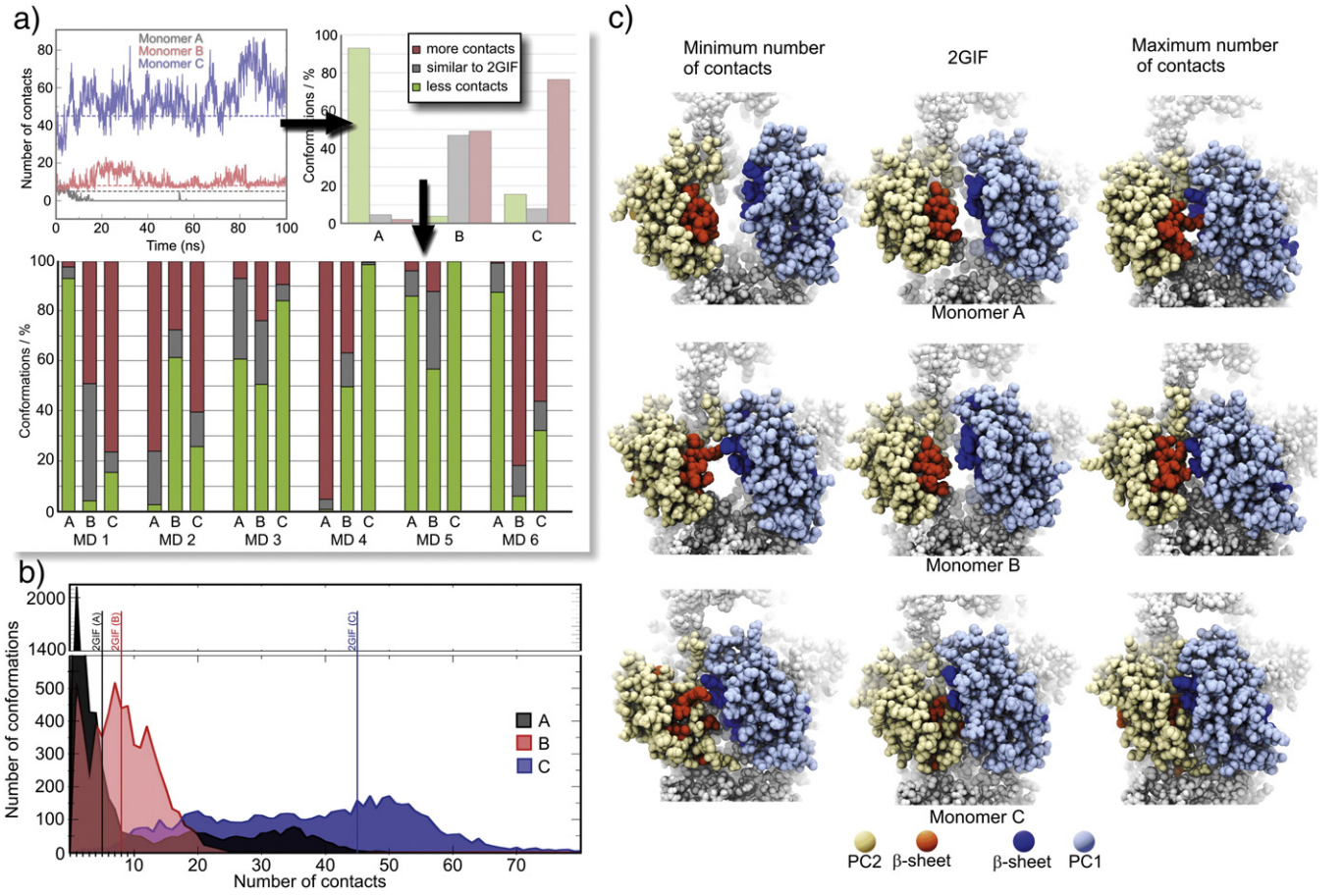

Fig. 4. Transport channel entrance PDe. To monitor the opening state of the porter domain transport channel entrances PDe we calculated the number of PC1–PC2 subdomain Cα-contacts within 1 nm. Computed for each monomer in each simulation (MD1–6), the number of Cα-contacts per frame was compared to the 2GIF crystal structure and classified into three groups of more, similar or less contacts than in the X-ray structure (a). Based on the overall distribution of PC1–PC2 contacts (b) extreme conformations were identified and compared to the PDe conformations seen in the X-ray structure (c).

distance distributions of TMD-Phe563 and PD-Thr676 α-carbons (Fig. 5b), we find that in all monomers a loop conformation close to the crystal structure is predominant permitting PD access in monomers A and B but not in C, with maxima in the Phe563–Thr676 Cα-distance distribution occurring either nearby or below the distance seen in the crystal structure.

3.2.2. Substrate channel exit PDx

In the exit regions of the substrate transportation channels, opening states in each monomer were monitored via the COM distances of the proposed gating residues Gln124 and Tyr758 [17] (Fig. 6a). Calculating percentage per-run occurrences (Fig. 6b) and overall COM distance distributions over all simulations (Fig. 6c, Table 1), we find that crystal structure-like or larger distances are predominant, displaying sharp, single peaks at 0.6 nm (monomer A) and 0.55 nm (monomer B) in the overall distribution. Monomer C shows a different behavior exhibiting two distance peaks at 0.75 and 1.8 nm corresponding to opening and closing motions of the channel exit not occurring in A and B as illustrated by representative A and B conformations (Fig. 6d,e) as well as extreme monomer C conformations based on the overall distance distributions (Fig. 6f,g).

To exclude possible artifacts arising from describing the opening state of a channel by a single distance only, we performed an additional analysis of the PDx opening state computing the triangular cross-sectional area (TCA) spanned by the centers of mass of Gln124, Tyr758 and Pro50 (supplemental Fig. 1a). While Gln124 and Tyr758 have been proposed as gating residues [17], we selected Pro50 due to its location near the channel exit and monomer-specific position shifts in the 2GIF AcrB crystal structure [9]. As evident from the (a) overall TCA distribution calculated over all simulations (supplemental Fig. 1b), and (b) the percentage per-run occurrence of monomer conformations exhibiting similar, lower or higher TCA than the 2GIF crystal structure (supplemental Fig. 1c), the TCA analysis yields the same results as the gating residue distance analysis. Whereas the proposed exit of the PD substrate transportation channel remains closed in monomers A and B, it opens and closes in monomer C.

Table 1
Porter domain transport channel opening states in percentage of total simulation time.

Monomer	Periplasmic cleft entrance			Exit		
	More open	Like 2GIF	More closed	More open	Like 2GIF	More closed
A	55	14	31	27	71	2
B	38	23	39	43	57	0
C	59	7	34	81	3	16

3.3. Opening state of the hydrophobic binding pocket

Once AcrB substrates have passed the “Phe617” or “switch loop” [15,16] they reach the “deep” or “hydrophobic binding pocket” [9,14–17]. Whereas in the available crystal structures the hydrophobic binding pocket is in an open conformation in monomer B, it is closed in monomers A and C [9,14–17]. To monitor the HBP opening state we computed for all monomers in all simulations the radius of gyration of the α-carbons of all HBP residues and compared it to the

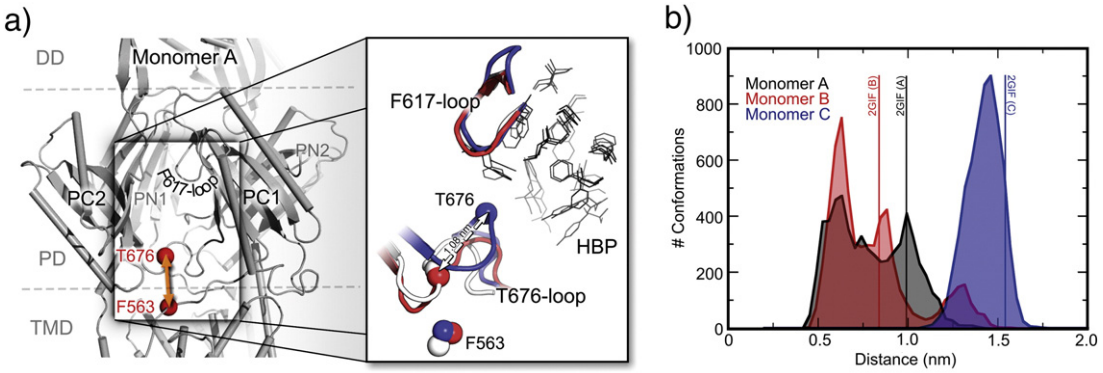

Fig. 5. Thr676 loop. Connecting the PC1 and PC2 subdomains, the Thr676 loop adopts monomer-specific conformations in the AcrB crystal structures (a). Displaying a membrane-facing Thr676 orientation in the L (monomer A, white) and T state (monomer B, red) permitting substrate passage, the loop conformation in the O state (monomer C, blue) is characterized by a 1 nm position shift of Thre676 towards the Phe617 or switch loop inhibiting substrate access to the porter domain. As monitored through the Thr676–Phe563 Cα distance distribution, the Thr676 loop predominantly adopts similar conformations through the MD simulations (b).

2GIF crystal structure (Fig. 7). Whereas in monomers A and C the HBP radius of gyration fluctuates around the 0.74 and 0.75 nm value of the crystal structure, in monomer B the radius of gyration drops from the initial 0.84 nm in the X-ray structure down to a range from 0.72 to 0.77 nm (Fig. 7a). As illustrated by HBP snapshots before (Fig. 7b) and after 100 ns simulation time the HBP collapses in monomer B (Fig. 7c).

3.4. Potential convergence of monomer conformations

To assess whether monomers become more similar to each other in the absence of substrate during the simulations we compared their conformations at each time frame of the trajectories. Monitoring the relative conformational PD-DD distances between monomers A and B compared to C as well as B compared to A, we calculated Cα RMSDs after least squares fitting each simulation frame to the respective monomers C and A conformation (Fig. 8a). In all cases the relative Cα RMSDs increase, exceeding in all runs the initial inter-monomeric conformational distances in the X-ray structure (Fig. 8a, horizontal lines) within the first 10 ns. Neither monomer A or B adopts a conformation more similar to C nor does monomer A become structurally similar to B throughout the simulations.

In 2008 Seeger and co-workers published a study using engineered disulfide bonds to analyze domain motions during the AcrB reaction cycle [11]. Among the numerous cysteine mutants investigated, the Ser562Cys and Thr837Cys double mutant was reported to act as an indicator for the "open/extrusion" monomer C conformation, which was found as the only conformation permitting the formation of a Cys562–Cys837 disulfide bond. To provide further evidence that the observed PDe closure in monomers A and B does not indicate a conformational transition towards the C state, we computed the distribution of Ser562–Thr837 Cα-distances over all six simulations (Fig. 8b). With distance peaks at 1.1 (monomer A), 1.3 (monomer B) and 0.6 nm (monomer C), only in monomer C Cα-distances below 0.638 nm occur which has been reported as the upper Cα-distance limit permitting the formation of a disulfide bond [43].

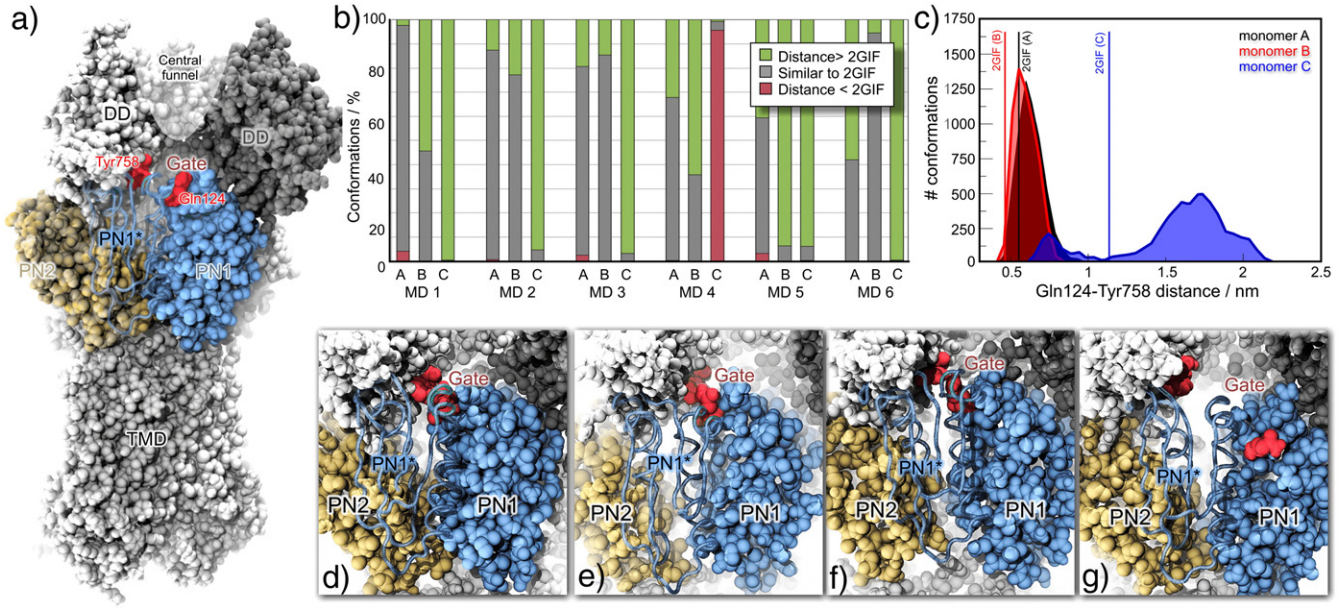

Fig. 6. Transport channel exit PDx. As illustrated by a cut-away view of monomer C, PDx faces the interior of the AcrB trimer and is flanked by the docking domain (DD) the PN1 subdomain and the PN1 subdomain of the adjacent protomer (PN1*) which is A in this case (a). Gln124 in the PN1 and Tyr758 in the N-terminal part of the docking domain (DD, white) have been proposed as gating residues. Monitoring the Gln124–Tyr758 center of mass distances we computed for each simulation the percentage occurrence of conformation displaying smaller, similar or larger distances as in the 2GIF X-ray structure (b). Based on the overall distribution of Gln124–Tyr758 distances (c) representative average (d, de) and extreme conformations (f, g) were selected. While closed in monomer A (d) and B (e), PDx opens and closes in monomer C (f, g).

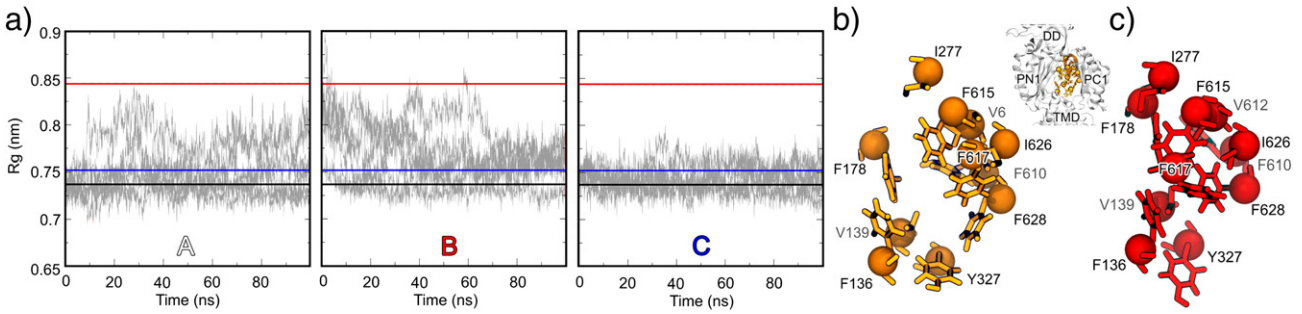

Fig. 7. Hydrophobic binding pocket. To monitor the opening state of the hydrophobic binding pocket (HBP) during our simulation we calculated the radius of gyration of the HBP residues' α carbons (a). While fluctuating around the crystal structure values in monomers A and C, the monomer B HBP radius of gyration decreases in simulations. As illustrated by snapshots of the monomer B HBP (b) and after 100 ns MD simulation (c), the binding pocket collapses.

3.5. Crystal vs. simulation average structure

Throughout our simulations AcrB adopts conformations which have not been reported in the published crystal structures [9,14–18] To provide possible evidence explaining this discrepancy we computed the simulation average structure over all simulations and compared it to the 2GIF crystal structure calculating Cα-RMSD and Cα-displacements after respective least squares fitting (supplemental Fig. 2a).

With an overall Cα-RMSD of 0.21 nm X-ray and simulation average structure are very similar. The largest displacements occur in the cytoplasmic loop connecting transmembrane helix (TM) 6 and helix Iα2 in monomers A, B and C, the C-terminus in monomer B, PC1 in monomers B, C, the cytoplasmic end of TM 4 in monomers B and A, the N-terminal half of the docking domain (DN) in monomers B, C, the C-terminal half of the docking domain (DC) in monomers B, C and A as well as in the middle of N-terminal PD subdomain PN1 in monomer B. To assess whether these differences stem from residue–residue interactions stabilizing the AcrB conformation in the X-ray crystal, we computed all residues involved in 0.4 nm crystal contacts in the 2GIF X-ray structure and compared these with residues in the simulation average structure exhibiting Cα-displacements of 0.4 nm or more (supplemental Fig. 2b). Residues involved in crystal contacts are shown in van der Waals representation whereas residues displaying maximum Cα-displacement appear as red sticks when not involved in crystal contacts or in red van der Waals representation when coinciding with crystal contacts. The majority of residues displaying maximum conformational deviation from the X-ray structure does not coincide with residues involved in 2GIF crystal contacts.

4. Discussion

Addressing the question whether the high level of monomer-characteristic similarity seen in the PD conformation of all AcrB crystal structures (Fig. 2) represents an intrinsic feature of the protein or could stem from other causes, we performed a series of 6×100 ns independent, unbiased molecular dynamics simulations of asymmetric AcrB in an explicit phospholipid membrane/water environment at 150 mM NaCl concentration. Monitoring the opening state of the entrance PDe and exit regions PDx of the PD substrate transport channels, we find changes in the number of inter-domain contacts (Fig. 4), the distance (Fig. 6) and triangular cross-sectional areas (supplemental Fig. 1) of proposed PDx gating residues suggesting that PDe opens and closes in monomers A and B but remains closed in C, whereas PDx remains closed in A and B but opens and closes in C. While one might argue that changes of these parameters do not necessarily indicate opening and closing motions, the extreme conformations based on the obtained data imply that at least under the simulated conditions PDe and PDx are more flexible than previously assumed based on the available AcrB crystal structures. We begin this section discussing the limitations of our approach, and then proceed to our findings and their biological implications.

4.1. Limitations of our approach

With any molecular dynamics simulation the question always arises whether simulation time was long enough in respect to the problem under investigation. Sampling different regions of conformational space in each run, in six independent and unbiased 100 ns MD simulations the AcrB structure did not converge (Fig. 3b) which was to be expected given the findings reported in [44] where 1.6 μs of atomistic MD simulation of membrane-embedded rhodopsin was not long enough for the protein to converge. Nevertheless we still consider the amount of conformational sampling achieved adequate given that (a) the aim of our study was to explore AcrB ground state dynamics near the crystal structure; (b) throughout the simulations the protein already visited unreported conformations (Figs. 4, 6, 7, supplemental

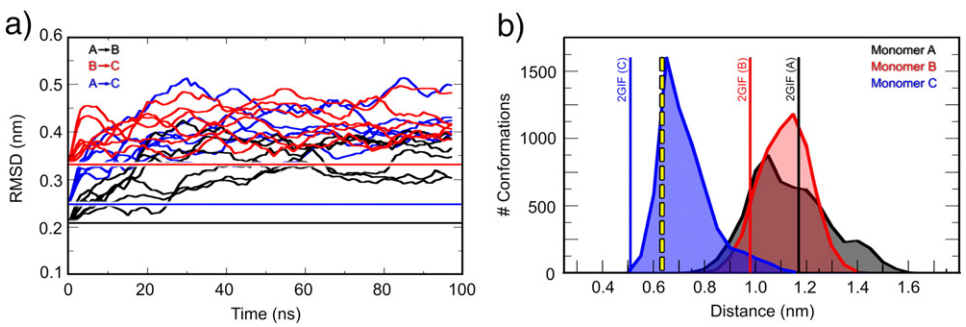

Fig. 8. Potential convergence of monomer conformations. As evident from relative Cα RMSDs comparing the conformational distances between the monomers throughout the simulations, the monomers do not adopt similar conformations in the absence of transport substrate (a). In an earlier study [11] the distance between TMD-Ser562 and PD-Thr837 has been identified as indicative for the monomer C state, permitting only here the formation of a disulfide bond when mutated to cysteine. As seen by the Ser562–Thr837 Cα distance distribution only in monomer C distances below 0.638 nm occur which has been reported as upper limit for the formation of disulfide bonds [43].

Fig. 1) which might provide potential inside into AcrB efflux pump mechanism as discussed below; and (c) our simulations represent the most extensive sampling of unbiased AcrB dynamics reported so far [31].

Another limitation that should be kept in mind regards the representation of the protein's micro-environment using a homogeneous POPE bilayer neglecting any other AcrB interaction partners such as AcrA, TolC or YajC [25,45–47]. Whereas the former approximation is common in simulating bacterial membrane proteins and justified by a natural occurrence of 75–85% POPE in the *E. coli* membranes [48], simulations assessing the influence of other AcrB interaction partners are currently under way in our lab.

4.2. Simulation and experiment

Throughout our simulations wild type AcrB adopts PD conformations which have not been reported in the published crystal structures [9,14–18]including closed PDe conformations in monomers A and B (Fig. 4), closed PDx conformations in C (Fig. 6, supplemental Fig. 1) as well as a collapsed hydrophobic binding pocket in monomer B (Fig. 7). A possible explanation why these conformations have not been detected yet could be that crystal packing limits the PD conformations to the ones observed in the X-ray structures so far (supplemental Fig. 2). However, the lack of overlap between residues displaying maximum Cα-displacements in the simulation average structure (supplemental Fig. 2b, red residues) and residues involved in 0.4 nm crystal contacts in the 2GIF X-ray structure (supplemental Fig. 2b, residues in van der Waals representation) speaks against crystal packing playing a major role in confining porter domain conformations. On the other hand, as protein is always crystallized in the presence of detergent and most detergents are AcrB substrates, it is also possible that bound but structurally unresolved substrate molecules might induce a more defined conformational state. As in our computer experiments AcrB is simulated outside a crystal environment in the absence of any substrate or detergent, the observed PDe and PDx dynamics (Figs. 4, 6, supplemental Fig. 1) as well as the collapse of the hydrophobic binding pocket in monomer B (Fig. 7) could be interpreted in favor of this hypothesis.

A key characteristic of monomer C is a closed PDe conformation in the available AcrB crystal structures (Fig. 2). Whereas the observed PDe closure in monomers A and B (Fig. 4) could indicate a conformational transition towards the C monomer, three observations speak against that hypothesis. For one, as indicated by relative Cα-RMSD analysis comparing the monomer conformations throughout each of the six trajectories (Fig. 8a), monomers A and B increase their conformational distance to monomer C in all simulations. Second, as reported in a previous combined mutagenesis/mass spectrometry study [11], the Ser562Cys/Thr837Cys double mutant can be used as a tool to identify protomer conformations, permitting the formation of a Cys562–Cys837 disulfide bond only in a monomer C. When calculating the distribution of Ser562–Thr837 Cα distances in our wild type AcrB simulations (Fig. 8b), we find that only in monomer C Cα distances below 0.638 nm occur which has been determined as the upper Cα distance limit permitting the formation of disulfide bonds in a previous analysis of high resolution protein X-ray structures [43]. This result puts our simulations in agreement with the experimental finding reported in [11] that under in vivo conditions only one AcrB protomer is in a conformation similar to monomer C. Third, next to the PDe opening state another conformational difference between the monomers in the AcrB crystal structures is the conformation of the Thr676 loop connecting the PC1 and PC2 subdomains, displaying a TMD-facing Thr676 orientation in monomers A and B but a switch loop-facing Thr676 orientation in monomer C where the threonine shifted by approximately 1 nm away from its position in A and B (Fig. 5a). If monomers A and B underwent transitions towards a conformation similar to monomer C, this would have to include a conformational change of the Thr676 loop. Using the Thr676–Phe563 Cα distance to monitor the loop conformation, we find, like in the X-ray structures, the loop favoring conformations with a TMD-facing Thr676 orientation in monomers A and B and a switch loop-facing Thr676 orientation in monomer C. (Fig. 5b).

If our simulations are correct our findings suggest that the high degree of monomer-specific conformational homogeneity seen in all AcrB crystal structures (Fig. 2) is not an intrinsic feature of the protein but an effect of the crystallization environment as discussed above. Testing this hypothesis experimentally could be done using for example double spin label electron spin resonance or fluorescence spectroscopy techniques to monitor the opening state of the PDe, whereas cross linking experiments could be employed to investigate PDx gating residue dynamics and intermediate-dependent position changes of Thr676.

4.3. Biological implications

4.3.1. Monomer conformations in the reaction cycle

Based on the available crystal structures, AcrB can adopt three different monomer conformations representing the reaction cycle intermediates *L*oose/access (monomer A), *T*ight/binding (monomer B) and *O*pen/extrusion (monomer C). Furthermore, two different trimeric AcrB structures are currently known, the asymmetric LTO conformation [9,14,17] and the symmetric LLL conformation [16,18]. If our simulations of membrane-embedded AcrB outside a crystal environment in the absence of any transport substrate are correct our findings suggest that each state occurs in at least two variants: L and T with open or closed PDe (Fig. 4) and O with open or closed PDx conformations (Fig. 6, supplemental Fig. 1). Although one might argue that some conformational PD flexibility is to be expected for the known monomer conformations, the scale of the observed PC1 and PC2 motions in the PDe region within the same intermediate clearly exceeds the conformational variation so far seen in any of the available 33 AcrB X-ray structures (Fig. 2). Against this background a further investigation of the questions whether the AcrB reaction cycle comprises more than three distinct monomer conformations or whether the intermediate definition currently employed might require revision seems reasonable.

Whereas the LTO state is interpreted as the lowest energy form of the AcrB trimer in the presence of substrate [16,22,27,49], the LLL state is regarded as representing a resting state in the absence of substrate [22]. If LLL is a substrate-free resting state the question arises why apparently ligand-free AcrB structures like 2GIF [9] show the trimer in LTO form. A possible answer could be bound but structurally unresolved substrate molecules as discussed in Section 4.2. If the hypothesis of AcrB adopting LLL conformations in the absence of substrate is correct one would assume that LTO AcrB would undergo conformational changes towards an LLL state once all substrate has been removed. During our simulations no such trend is observed. Although representing the longest sample of unbiased, membrane-embedded AcrB dynamics currently available [28–31] one could argue that 100 ns is rather short and the necessary transitions towards uniform monomer conformations occur on longer time scales. However, the observation that in all our simulations the conformational distances between the three monomers increase (Fig. 8a) could be interpreted as piece of evidence speaking against an LLL resting state.

4.3.2. Substrate binding and transport

So far substrate binding to AcrB has been observed for the L and the T state, involving an outer, “proximal” or “access” binding pocket which is equivalent to the PDe in our simulations and an inner, “distal”, “deep” or “hydrophobic binding pocket” (HBP) separated by a “switch” or “Phe617” loop [15,16]. Based on the observed binding behavior of differently sized substrate molecules to the L and T monomers [15,16], it has been concluded that substrate binding is a size-dependent process. Whereas small substrates either accumulate in the outer proximal

binding pocket or reach the inner hydrophobic binding pocket by self-diffusion, larger substrates require protein conformational transitions as part of the AcrB reaction cycle in order to reach the inner, hydrophobic binding pocket [15,16]. Once there, all substrates require reaction cycle-induced conformational changes to be expelled into the central funnel formed by the AcrB docking domain leading towards TolC [49].

In general agreement with the proposed transport mechanism our simulations of membrane-embedded, substrate-free AcrB add three new aspects to this scenario. First, in the absence of substrate the inner hydrophobic binding pocket collapses in T while remaining predominantly closed in L and O (Fig. 7). Beyond providing another piece of evidence speaking for the presence of unresolved, LTO-stabilizing compounds in the 2GIF crystal structure, the question arises how easily the hydrophobic binding pocket reopens when substrate arrives. Can small substrates indeed merely self-diffuse into the HBP as suggested in [15] or do they too require reaction cycle-induced changes of the PD conformation to be actively pushed into the closed HBP? Computational experiments addressing this question simulating the binding of small and large substrate species are currently underway in our lab. Second, adopting conformations permitting PD access in L and T but blocking it in O in the AcrB crystal structures [9,14–17], the Thr676 loop seems to be involved in regulating PD access together with the relative orientation of the PC1 and PC2 subdomains (Fig. 5a). Whereas the crystal structures suggest that the Thr676 loop conformation is coupled to the motion of the PC1 and PC2 subdomains, our analysis of the Thr676–Phe563 Cα distances indicates an independency of both structural elements with the Thr676 loop favoring conformations close to its L/T or O opening state as seen in the X-ray structure regardless whether the subdomains are open or closed (Figs. 5b, 4b and c). Apparently requiring the energy of a T to O transition in the AcrB reaction cycle to change conformation, the Thr676 loop could also play an active role in pushing substrates towards the deep hydrophobic binding pocket based on our simulation findings. Confining Thr676 loop conformations in cross-linking studies combined with AcrB activity measurements could provide a possible means to test this hypothesis experimentally. Third, the Gln124/Tyr758 dynamics observed in our simulations leading to the opening and closure of the PDx towards the central funnel of the docking domain (Fig. 6, supplemental Fig. 1) support the proposed gating function of these residues [17].

4.3.3. Possible influence of porter domain dynamics on pump activity

If our simulations are correct, three possible effects on pump activity are conceivable for a toxin exporter whose substrate-accessible intermediates switch between conformations permitting and blocking substrate binding. (1) PDe opening and closing enhances AcrB pump activity for example by generating a directed water flow which could play a role in the proposed peristaltic pump mechanism [9,11,12,17,18,50] assisting in attracting substrates or pushing them towards the inner distal binding pocket. Simulating the AcrB conformational cycle using targeted MD techniques [51] such a water flow has been reported in [30]. Alternatively the observed PDe dynamics could also provide the structural basis for a cleaning mechanism of the transport channel entrance expulsing molecules that AcrB cannot be transported as proposed in [27,49]. (2) PDe opening and closing has no effect on the AcrB pump activity and the substrate-accessible porter domain occurs in a dynamic equilibrium of open and closed PDe similar to the second functional model of Venus flytrap mechanism in periplasmic binding proteins [52,53]. (3) PDe opening and closing hinders pump activity by lowering the life time of substrate-accessible open PDe states.

A possible way to test these hypotheses experimentally could be through PC1–PC2 distance measurements via fluorescence or double spin label electron spin resonance spectroscopy performed on isolated AcrB as well as in the presence of AcrA and Mg^{2+} which are known to enhance AcrB pump activity [7]. Next to the principal check whether PDe opening and closing occurs outside in silico conditions as discussed in Section 4.2., similar distance distributions would speak in favor of the neutral effect on pump activity, whereas broader distance distributions in the AcrB–AcrA–Mg^{2+} scenario would support a positive influence on AcrB activity. Conversely, a smaller distance distribution under AcrB–AcrA–Mg^{2+} conditions would imply a negative effect of PDe opening and closing. If that was the case this observation could be interpreted as a stabilizing effect AcrA enacts on the PDe conformations which could in turn provide a structural explanation for the activity-enhancing effect of adaptor protein: without AcrA the PDe opens and closes and the life time of substrate-accessible i.e. open conformations is reduced. Conversely, if AcrA indeed stabilizes open PDe conformations, the life time of substrate-accessible open PDe conformations is increased. While on the other hand a PDe dynamics-enhancing effect of AcrA is principally also conceivable, this option appears less likely given the close contact between inner membrane transporter and adaptor protein observed recently in the crystal structure of the homologue heavy metal efflux pump CusA in complex with its adaptor protein CusB [54] but is also seen between AcrA and PC1 AcrB subdomain in the currently best available docking model of the assembled AcrAB–TolC complex based on biochemical cross linking data [47]. Either way it will be exciting to see the question and relevance of porter domain dynamics in AcrB and other RND inner membrane transporters investigated further both experimentally and computationally in the presence and absence of other efflux pump components. Simulations assessing the influence of both TolC and AcrA are currently underway in our lab.

5. Conclusions

Addressing the question why all AcrB crystal structures display nearly identical porter domain conformations in the same reaction cycle intermediate we performed a series of six independent, unbiased 100 ns molecular dynamics simulations of membrane-embedded asymmetric AcrB in the absence of any substrate. The conformational dynamics we observed indicate that the porter domain is more flexible than previously assumed displaying clear opening and closing motions of the proximal binding pocket and the exit regions of the drug transport channels while the distal hydrophobic pocket favors a closed conformation in all three protomers. If our simulations are correct our findings suggest that the conformational homogeneity seen in the crystal structures is likely not an intrinsic feature of AcrB but an artifact caused by bound but structurally unresolved buffer or detergent molecules. Furthermore our findings imply that each of the currently known three reaction cycle intermediates occurs in at least two variants and that beyond independently regulating porter domain access the Thr676 loop could play a key role in substrate transport pushing compounds towards the hydrophobic binding pocket. On a 100 ns time scale we find no conformational trends indicating the proposed transition towards homogeneous, resting state-like protomer conformations in the absence of substrate. If the proximal binding pocket dynamics have an inhibiting effect on AcrB pump activity by lowering the life time of substrate-accessible conformations, the observed opening and closing motions in the isolated protein could provide a structural explanation for the AcrB-enhancing effect of the adaptor protein AcrA stabilizing PC1 and PC2 subdomain orientations.

Acknowledgements

We thank Martin Raunest and Thomas H. Schmidt for proofreading and helpful comments. This work was financially supported by the Ministerium für Innovation, Wissenschaft und Forschung des Landes Nordrhein-Westfalen. ChK is a junior research group leader funded by the NRW Rückkehrerprogramm.

Appendix A. Supplementary data

Supplementary data to this article can be found online at http://dx.doi.org/10.1016/j.bbamem.2012.10.016.

References

[1] X.Z. Li, H. Nikaido, Efflux-mediated drug resistance in bacteria: an update, Drugs 69 (2009) 1555–1623.
[2] H. Nikaido, Multidrug resistance in bacteria, Annu. Rev. Biochem. 78 (2009) 119–146.
[3] E. Lautenbach, J.P. Metlay, X. Mao, X. Han, N.O. Fishman, W.B. Bilker, P. Tolomeo, M. Wheeler, I. Nachamkin, The prevalence of fluoroquinolone resistance mechanisms in colonizing *Escherichia coli* isolates recovered from hospitalized patients, Clin. Infect. Dis. 51 (2010) 280–285.
[4] I.T. Paulsen, J.H. Park, P.S. Choi, M.H. Saier Jr., A family of Gram-negative bacterial outer membrane factors that function in the export of proteins, carbohydrates, drugs and heavy metals from Gram-negative bacteria, FEMS Microbiol. Lett. 156 (1997) 1–8.
[5] T. Dinh, I.T. Paulsen, M.H. Saier Jr., A family of extracytoplasmic proteins that allow transport of large molecules across the outer membranes of gram-negative bacteria, J. Bacteriol. 176 (1994) 3825–3831.
[6] D. Ma, D.N. Cook, M. Alberti, N.G. Pon, H. Nikaido, J.E. Hearst, Molecular cloning and characterization of AcrA and AcrE genes of *Escherichia coli*, J. Bacteriol. 175 (1993) 6299–6313.
[7] H.I. Zgurskaya, H. Nikaido, Bypassing the periplasm: reconstitution of the AcrAB multidrug efflux pump of *Escherichia coli*, Proc. Natl. Acad. Sci. U. S. A. 96 (1999) 7190–7195.
[8] H.I. Zgurskaya, H. Nikaido, AcrA is a highly asymmetric protein capable of spanning the periplasm, J. Mol. Biol. 285 (1999) 409–420.
[9] M.A. Seeger, A. Schiefner, T. Eicher, F. Verrey, K. Diederichs, K.M. Pos, Structural asymmetry of AcrB trimer suggests a peristaltic pump mechanism, Science 313 (2006) 1295–1298.
[10] M.A. Seeger, K. Diederichs, T. Eicher, L. Brandstatter, A. Schiefner, F. Verrey, K.M. Pos, The AcrB efflux pump: conformational cycling and peristalsis lead to multidrug resistance, Curr. Drug Targets 9 (2008) 729–749.
[11] M.A. Seeger, C. von Ballmoos, T. Eicher, L. Brandstätter, F. Verrey, K. Diederichs, K.M. Pos, Engineered disulfide bonds support the functional rotation mechanism of multidrug efflux pump AcrB, Nat. Struct. Mol. Biol. 15 (2008) 199–205.
[12] Y. Takatsuka, H. Nikaido, Covalently linked trimer of the AcrB multidrug efflux pump provides support for the functional rotating mechanism, J. Bacteriol. 191 (2009) 1729–1737.
[13] H. Nikaido, Y. Takatsuka, Mechanisms of RND multidrug efflux pumps, Biochim. Biophys. Acta 1794 (2009) 769–781.
[14] S. Murakami, R. Nakashima, E. Yamashita, T. Matsumoto, A. Yamaguchi, Crystal structures of a multidrug transporter reveal a functionally rotating mechanism, Nature 443 (2006) 173–179.
[15] R. Nakashima, K. Sakurai, S. Yamasaki, K. Nishino, A. Yamaguchi, Structures of the multidrug exporter AcrB reveal a proximal multisite drug-binding pocket, Nature 480 (2011) 565–569.
[16] T. Eicher, H.J. Cha, M.A. Seeger, L. Brandstätter, J. El-Delik, J.A. Bohnert, W.V. Kern, F. Verrey, M.G. Grütter, K. Diederichs, K.M. Pos, Transport of drugs by the multidrug transporter AcrB involves an access and a deep binding pocket that are separated by a switch-loop, PNAS 109 (2012) 5687–5692.
[17] G. Sennhauser, P. Amstutz, C. Briand, O. Storchenegger, M.G. Grütter, Drug export pathway of multidrug exporter AcrB revealed by DARPin inhibitors, PLoS Biol. 5 (2007) e7.
[18] S. Murakami, R. Nakashima, E. Yamashita, A. Yamaguchi, Crystal structure of bacterial multidrug efflux transporter AcrB, Nature 419 (2002) 587–593.
[19] E.W. Yu, J.R. Aires, H. Nikaido, AcrB multidrug efflux pump of *Escherichia coli*: composite substrate-binding cavity of exceptional flexibility generates its extremely wide substrate specificity, J. Bacteriol. 185 (2003) 5657–5664.
[20] E.W. Yu, G. McDermott, H.I. Zgurskaya, H. Nikaido, D.E. Koshland, Structural basis of multiple drug-binding capacity of the AcrB multidrug efflux pump, Science 300 (2003) 976–980.
[21] E.W. Yu, J.R. Aires, G. McDermott, H. Nikaido, A periplasmic drug-binding site of the AcrB multidrug efflux pump: a crystallographic and site-directed mutagenesis study, J. Bacteriol. 187 (2005) 6804–6815.
[22] C.C. Su, M. Li, R. Gu, Y. Takatsuka, G. McDermott, H. Nikaido, E.W. Yu, Conformation of the AcrB multidrug efflux pump in mutants of the putative proton relay pathway, J. Bacteriol. 188 (2006) 7290–7296.
[23] D. Das, Q.S. Xu, J.Y. Lee, I. Ankoudinova, C. Huang, Y. Lou, A. DeGiovanni, R. Kim, S.H. Kim, Crystal structure of the multidrug efflux transporter AcrB at 31 Å resolution reveals the N-terminal region with conserved amino acids, J. Struct. Biol. 158 (2007) 494–502.
[24] D. Drew, M.M. Klepsch, S. Newstead, R. Flaig, J.W. De Gier, S. Iwata, K. Beis, The structure of the efflux pump AcrB in complex with bile acid, Mol. Membr. Biol. 25 (2008) 677–682.
[25] S. Tornroth-Horsefield, P. Gourdon, R. Horsefield, L. Brive, N. Yamamoto, H. Mori, A. Snijder, R. Neutze, Crystal structure of AcrB in complex with a single transmembrane subunit reveals another twist, Structure 15 (2007) 1663–1673.
[26] W.C. Lu, C.Z. Wang, E.W. Yu, K.M. Ho, Dynamics of the trimeric AcrB transporter protein inferred from a B-factor analysis of the crystal structure, Proteins 62 (2006) 152–158.
[27] X.Q. Yao, H. Kenzaki, S. Murakami, S. Takada, Drug export and allosteric coupling in a multidrug transporter revealed by molecular simulations, Natl. Commun. 1 (2010) 117.
[28] A.V. Vargiu, F. Collu, R. Schulz, K.M. Pos, M. Zacharias, U. Kleinekathöfer, P. Ruggerone, Effect of the F610A mutation on substrate extrusion in the AcrB transporter: explanation and rationale by molecular dynamics simulations, J. Am. Chem. Soc. 133 (2011) 10704–10707.
[29] R. Schulz, A.V. Vargiu, F. Collu, U. Kleinekathöfer, P. Ruggerone, Functional rotation of the transporter AcrB: insights into drug extrusion from simulations, PLoS Comput. Biol. 6 (2010).
[30] R. Schulz, A.V. Vargiu, P. Ruggerone, U. Kleinekathöfer, Role of water during the extrusion of substrates by the efflux transporter AcrB, J. Phys. Chem. B 115 (2011) 8278–8287.
[31] N. Fischer, C. Kandt, Three ways in, one way out: water dynamics in the trans-membrane domains of the inner membrane translocase AcrB, Proteins 79 (2011) 2871–2885.
[32] H.J.C. Berendsen, D. van der Spoel, R. van Drunen, GROMACS: a message-passing parallel molecular dynamics implementation, Comput. Phys. Commun. 91 (1995) 43–56.
[33] B. Hess, C. Kutzner, D. van der Spoel, E. Lindahl, GROMACS 4: algorithms for highly efficient, load-balanced, and scalable molecular simulation, J. Chem. Theory Comput. 4 (2008) 435–447.
[34] C. Oostenbrink, A. Villa, A.E. Mark, W.F. van Gunsteren, A biomolecular force field based on the free enthalpy of hydration and solvation: the GROMOS force-field parameter sets 53A5 and 53A6, J. Comput. Chem. 25 (2004) 1656–1676.
[35] J. Pan, D.P. Tieleman, J.F. Nagle, N. Kucerka, S. Tristram-Nagle, Alamethicin in lipid bilayers: combined use of X-ray scattering and MD simulations, Biochim. Biophys. Acta 1788 (2009) 1387–1397.
[36] H.J.C. Berendsen, J.P.M. Postma, W.F. Vangunsteren, J. Hermans, Interaction models for water in relation to protein hydration, in: B. Pullman (Ed.), Intermolecular Forces, Reidel, Dordrecht, 1981, pp. 331–342.
[37] H.J.C. Berendsen, J.P.M. Postma, W.F. van Gunsteren, A. DiNola, J.R. Haak, Molecular dynamics with coupling to an external bath, J. Chem. Phys. 81 (1984) 3684.
[38] T. Darden, D. York, L. Pedersen, Particle mesh Ewald: an N·log(N) method for Ewald sums in large systems, J. Chem. Phys. 98 (1993) 10089.
[39] U. Essmann, L. Perera, M.L. Berkowitz, T. Darden, H. Lee, L.G. Pedersen, A smooth particle mesh Ewald method, J. Chem. Phys. 103 (1995) 8577–8593.
[40] B. Hess, H. Bekker, H.J.C. Berendsen, J.G.E.M. Fraaije, LINCS: a linear constraint solver for molecular simulations, J. Comput. Chem. 18 (1997) 1463–1472.
[41] M. Raunest, C. Kandt, Locked on one side only: ground state dynamics of the outer membrane efflux duct TolC, Biochemistry 51 (2012) 1719–1729.
[42] R. Schulz, U. Kleinekathöfer, Transitions between closed and open conformations of TolC: the effects of ions in simulations, Biophys. J. 96 (2009) 3116–3125.
[43] B. Schmidt, L. Ho, P.J. Hogg, Allosteric disulfide bonds, Biochemistry 45 (2006) 7429–7433.
[44] A. Grossfield, D.M. Zuckerman, Quantifying uncertainty and sampling quality in biomolecular simulations, Annu. Rep. Comput. Chem. 5 (2009) 23–48.
[45] V. Koronakis, A. Sharff, E. Koronakis, B. Luisi, C. Hughes, Crystal structure of the bacterial membrane protein TolC central to multidrug efflux and protein export, Nature 405 (2000) 914–919.
[46] J. Mikolosko, K. Bobyk, H.I. Zgurskaya, P. Ghosh, Conformational flexibility in the multidrug efflux system protein AcrA, Structure 14 (2006) 577–587.
[47] M.F. Symmons, E. Bokma, E. Koronakis, C. Hughes, V. Koronakis, The assembled structure of a complete tripartite bacterial multidrug efflux pump, Proc. Natl. Acad. Sci. U. S. A. 106 (2009) 7173–7178.
[48] C.R. Raetz, Enzymology, genetics, and regulation of membrane phospholipid synthesis in *Escherichia coli*, Microbiol. Rev. 42 (1978) 614–659.
[49] K.M. Pos, Drug transport mechanism of the AcrB efflux pump, Biochim. Biophys. Acta 1794 (2009) 782–793.
[50] Y. Takatsuka, H. Nikaido, Site-directed disulfide cross-linking shows that cleft flexibility in the periplasmic domain is needed for the multidrug efflux pump AcrB of *Escherichia coli*, J. Bacteriol. 189 (2007) 8677–8684.
[51] J. Schlitter, M. Engels, P. Krüger, Targeted molecular dynamics: a new approach for searching pathways of conformational transitions, J. Mol. Graph. 12 (1994) 84–89.
[52] B.H. Oh, J. Pandit, C.H. Kang, K. Nikaido, S. Gokcen, G.F. Ames, S.H. Kim, Three-dimensional structures of the periplasmic lysine/arginine/ornithine-binding protein with and without a ligand, J. Biol. Chem. 268 (1993) 11348–11355.
[53] C. Kandt, Z. Xu, D.P. Tieleman, Opening and closing motions in the periplasmic vitamin B12 binding protein BtuF, Biochemistry 45 (2006) 13284–13292.
[54] C.C. Su, F. Long, M.T. Zimmermann, K.R. Rajashankar, R.L. Jernigan, E.W. Yu, Crystal structure of the CusBA heavy-metal efflux complex of *Escherichia coli*, Nature 470 (2011) 558–562.
[55] M. Petřek, M. Otyepka, P. Banáš, P. Košinová, J. Koča, J. Damborský, CAVER: a new tool to explore routes from protein clefts, pockets and cavities, BMC Bioinformatics 7 (2006) 316.